Effects of increasing the category resolution of the sea ice thickness distribution in a coupled climate model on Arctic and Antarctic sea ice

Madison Margaret Smith[1], Marika M Holland[2], Alek Aaron Petty[3], Bonnie Light[4], and David Anthony Bailey[2]

[1]University of Washington
[2]National Center for Atmospheric Research (UCAR)
[3]University of Maryland, College Park
[4]University of Washigton

November 22, 2022

Abstract

Many modern sea ice models used in global climate models represent the subgrid-scale heterogeneity in sea ice thickness with an ice thickness distribution (ITD), which improves model realism by representing the significant impact of the high spatial heterogeneity of sea ice thickness on thermodynamic and dynamic processes. Most models default to five thickness categories. However, little has been done to explore the effects of the resolution of this distribution (number of categories) on sea-ice feedbacks in a coupled model framework and resulting representation of the sea ice mean state. Here, we explore this using sensitivity experiments in CESM2 with the standard five ice thickness categories and fifteen ice thickness categories. Increasing the resolution of the ITD in a run with preindustrial climate forcing results in substantially thicker Arctic sea ice year-round. Analyses show that this is a result of the ITD influence on ice strength. With 15 ITD categories, weaker ice occurs for the same average thickness, resulting in a higher fraction of ridged sea ice. In contrast, the higher resolution of thin ice categories results in enhanced heat conduction and bottom growth and leads to only somewhat increased winter Antarctic sea ice. The spatial resolution of the ICESat-2 satellite mission provides a new opportunity to compare model outputs with observations of seasonal evolution of the ITD in the Arctic (ICESat-2; 2018-2021). Comparisons highlight significant differences from the ITD modeled with both runs over this period, likely pointing to underlying issues contributing to the representation of average thickness.

Effects of increasing the category resolution of the sea ice thickness distribution in a coupled climate model on Arctic and Antarctic sea ice

Madison M. Smith[1], Marika M. Holland[2], Alek A. Petty[3], Bonnie Light[1], David A. Bailey[2]

[1]Polar Science Center, Applied Physics Laboratory, University of Washington, Seattle, USA
[2]National Center for Atmospheric Research, Boulder, Colorado, USA
[3]Cryospheric Sciences Laboratory, NASA Goddard Space Flight Center, Greenbelt, MD, USA

Key Points:

- Higher resolution of the sea ice thickness distribution increases simulated Arctic sea ice thickness, with little change in Antarctic sea ice
- The impact has a bigger effect on dynamic processes than thermodynamic processes
- Comparison with subgrid-scale thickness observations from ICESat-2 suggests targeting ridging for improvement

Corresponding author: Madison M. Smith, `mmsmith@uw.edu`

Abstract

Many modern sea ice models used in global climate models represent the subgrid-scale heterogeneity in sea ice thickness with an ice thickness distribution (ITD), which improves model realism by representing the significant impact of the high spatial heterogeneity of sea ice thickness on thermodynamic and dynamic processes. Most models default to five thickness categories. However, little has been done to explore the effects of the resolution of this distribution (number of categories) on sea-ice feedbacks in a coupled model framework and resulting representation of the sea ice mean state. Here, we explore this using sensitivity experiments in CESM2 with the standard five ice thickness categories and fifteen ice thickness categories. Increasing the resolution of the ITD in a run with preindustrial climate forcing results in substantially thicker Arctic sea ice year-round. Analyses show that this is a result of the ITD influence on ice strength. With 15 ITD categories, weaker ice occurs for the same average thickness, resulting in a higher fraction of ridged sea ice. In contrast, the higher resolution of thin ice categories results in enhanced heat conduction and bottom growth and leads to only somewhat increased winter Antarctic sea ice. The spatial resolution of the ICESat-2 satellite mission provides a new opportunity to compare model outputs with observations of seasonal evolution of the ITD in the Arctic (ICESat-2; 2018-2021). Comparisons highlight significant differences from the ITD modeled with both runs over this period, likely pointing to underlying issues contributing to the representation of average thickness.

Plain Language Summary

The sea ice thickness is a key property of the sea ice cover, and is highly variable across the Arctic. The thickness influences thermal processes like growth and melt and dynamic processes like ridging. One of the simplifying assumptions that is applied in simulating sea ice in global climate models is representing the variation in ice thickness with an ice thickness distribution with a set number of categories. Typically, most models use five categories. Here, we test the impact of using a higher number of categories (15) on the simulation of sea ice. More ITD categories in the model results in significantly more simulated Arctic sea ice. This is primarily because the model estimates that the ice is weaker and so more of it is ridged into thicker ice. Modeled ice thickness distributions are also compared with thicknesses from satellite observations (ICESat-2). In the current version of the model, increasing the resolution of thickness does not improve the comparison with observations. We highlight areas for development and future work.

1 Introduction

Sophisticated sea ice models included in the current suite of global climate models now generally represent many of the dynamic and thermodynamic processes important for simulating the mean state of sea ice across both hemispheres. Various simplifications are invoked in order to account for the small-scale variability of the ice pack. For example, at the subgrid-scale level, the range of sea ice thickness is often represented using a discretized ice thickness distribution (ITD). The ITD defines the fraction of the ice cover with thicknesses in the range of specified bins (Figure 1). The idea of an ITD was first introduced by Thorndike et al. (1975) and adapted for climate models by C. M. Bitz et al. (2001), incorporating the mechanical redistribution proposed by Flato and Hibler III (1995). In the ITD formulation, sea ice is transferred between thickness categories as a result of simulated thermodynamic (e.g., growth and melt), and dynamic (e.g., ridging) processes. The ITD discretization then provides a computationally efficient means of parameterizing small-scale sea ice variability in models, with significant advantages over the use of a single mean grid-cell thickness.

Many parameterization schemes included in sea ice models are sensitive to the use of an ITD and the details of its resolution (C. M. Bitz et al., 2001; Holland et al., 2001). In fact, Massonnet et al. (2018) suggests that the main differences in the sea ice cover simulated by different global climate models are a result of varying ice thickness distribution schemes, as the thermodynamics schemes are generally quite similar. Fundamentally, thin ice grows faster than thicker ice and so exerts an unequal influence on ice growth, atmospheric heat fluxes, and brine rejection compared to thicker ice (Maykut, 1982). The relationship between growth and thickness is not linear, such that higher resolution of thin ice results in more growth and a thicker average ice cover (Holland & Curry, 1999). The resulting ice pack is also impacted by the influence of thickness on sea ice strength, where thin, first-year ice is weaker and more likely to participate in ridging (e.g., Flato & Hibler III, 1995). These processes can have cascading effects on the ice-ocean-atmosphere system (C. M. Bitz et al., 2001).

In most global climate models with an ITD, the default setting of five thickness categories originally proposed by C. M. Bitz et al. (2001) to capture the primary impacts of sea ice for the climate has largely been used without further investigation (Keen et al., 2021). However, more recent studies using a coupled ice-ocean model (NEMO-LIM) have investigated the impact of the number and bounds of ice thickness category discretization on the representation of global sea ice. Massonnet et al. (2011) found that increasing the number of ITD categories improved the seasonal to interannual variability of Arctic sea ice extent and retreat at basin-scales. In contrast, Moreno-Chamarro et al. (2020) found that increasing the number of thin categories resulted in worse comparisons of Arctic sea ice concentration and extent with observations when all other model settings were kept constant. Massonnet et al. (2019) more broadly investigated the impact of the discretization and resolution of thick ice categories on representation of sea ice over the historical period. However, to our knowledge there has not been any specific investigations into how increasing the number of ice thickness distribution categories might affect the representation of specific sea ice processes, particularly in a fully-coupled climate model with an interactive atmosphere. Additionally, despite the importance of sub-grid properties on key sea ice processes, prior studies examining model sensitivity to the ITD have focused on improving the comparison of mean state variables with observations, including total extent, total volume, and average thickness. There are only a few examples of studies in general that have examined the spatial variability or distribution of grid-cell mean thicknesses (e.g., Jahn et al., 2012), and there are no studies to our knowledge investigating subgrid-scale thickness distributions.

The main objective of this study is to examine the sensitivity of the sea ice state to increased resolution of the ITD. Our approach here improves on earlier analyses in two primary ways. First, the use of a fully-coupled framework, which allows for feedbacks and a more realistic representation of the ITD category resolution on sea ice, supports a focus on the impact of key physical processes on subgrid-scale thickness. Second, the use of new high-resolution sea ice observations allows us to assess comparisons of the subgrid-scale variability. We will begin by exploring the impact on Arctic and Antarctic sea ice mean state in a preindustrial control climate as a result of the differences in regime. We then investigate the possible implications for model realism by comparing model results from a current-day climate scenario with high spatial resolution ice thickness observations from ICESat-2. Our comparison with observations is possibly the first to evaluate modeled sea ice thickness on a subgrid-scale level. We suggest that evaluating the distribution of ice thickness in global climate models can provide insight into representation of processes beyond the typical comparison of mean state variables.

2 Model and Experimental Design

2.1 Coupled climate model configuration (CESM2-CAM6)

To investigate the role of the ITD category resolution in a coupled climate model, we perform simulations using the Community Earth System Model 2 (CESM2; Danabasoglu et al., 2020). We run CESM2 over a global domain with ocean and sea ice models on a displaced pole grid with a nominal horizontal resolution of 1° x 1°. CESM2 includes the sea ice model CICE version 5.1.2 (E. C. Hunke et al., 2015; E. Hunke et al., 2017). Information on the implementation of the sea ice model within CESM2 can be found in Bailey et al. (2020). The only significant change in the implementation here is the use of tuned albedos of snow on sea ice to give a realistic simulation of ice thickness over the historical period (Kay et al., 2022, ;details on tuning therein).

The CICE model includes an ice thickness distribution (Holland et al., 2006), which is common across most modern global sea ice models (Keen et al., 2021). Sea ice is discretized into a set number of categories (typically five), which occupy an evolving fraction of the grid cell. Sea ice volume and area are transferred between categories as a result of melt, growth, and dynamic processes. Lipscomb (2001) introduced a linear remapping scheme to transfer ice between categories, which has faster convergence than prior schemes. Linear remapping is also less diffusive, where more diffusive schemes can act to artificially smear out peaks in the distribution. The boundaries of the discretized ice thickness categories are determined following Lipscomb (2001, Eq. 22), which defines boundaries between 0 and 10 m using a tanh function to give wider spacing for increasing ice thickness. The minimum thickness of the thinnest category is set at 0.01 m. Greater category resolution for thin ice is beneficial to better resolve sea ice growth, which is a nonlinear function of ice thickness. Relatedly, poor resolution of thin ice categories can also result in more numerical diffusion.

The dynamic component of the CICE model utilizes the sea ice strength parameterization defined by Rothrock (1975). In this formulation, the sea ice strength is defined in proportion to the change in potential energy per unit of compressive deformation of the ice (Rothrock, 1975). The deformational work of compression goes into ridge-building (Flato & Hibler III, 1995). This is in contrast to the Hibler (1979) strength formulation used by many other sea ice models, where strength depends only on mean concentration and thickness. The Rothrock (1975) formulation results in a weaker icepack with higher resolution of the ITD (C. M. Bitz et al., 2001), likely because there are important physical effects that are not properly included (Ungermann et al., 2017). A thorough evaluation of the role of the strength parameterization on sea ice mean state sensitivity to the ITD is presented by Ungermann et al. (2017).

For this study, we perform simulations in preindustrial, historical and SSP3-7.0 scenarios, and primarily assess outputs from the preindustrial and SSP3-7.0 runs. Preindustrial runs were branched after 880 years with inter-annually invariant atmospheric conditions appropriate for year 1850. Preindustrial control runs were 60 years long, and averages and analysis were done over the last 25 years to investigate changes in processes. A run over the historical period with the relevant changes was initialized at the year 1850. This was then used to initialize an SSP3-7.0 experiment run at the year 2015, which is compared to four SSP3-7.0 ensemble members run over the same period, as described by Kay et al. (2022). These SSP3-7.0 runs are used for comparison with current satellite data.

All runs use the full atmosphere, sea ice, and land models of CESM2. The historical and future scenario also use the full dynamic ocean model, while the preindustrial runs use a simplified slab ocean model (SOM; C. M. Bitz et al., 2012). The SOM is used for preindustrial runs as it converges much faster (e.g., in around 20 years with CO_2 doubling) and so requires significantly less computational time. The ocean model is simplified to use fixed dynamic forcings and specified global mixed layer depths (with a minimum of 10 m depth). The temperature of the slab mixed layer is calculated using surface energy fluxes and a prescribed ocean heat flux associated with advection and mixing. Although dynamic feedbacks between the sea ice and ocean are limited by the use of the SOM in preindustrial runs, coupled climate feedbacks are generally well-captured (e.g., Bacmeister et al., 2020).

2.2 Sensitivity experiments

To examine the impact of ITD category resolution, we compare experimental runs with the default of 5 ITD categories with runs using an increased resolution of 15 ITD categories (Figure 1). The categories are preferentially distributed toward the thin classes following the default discretization scheme described above (Lipscomb, 2001, Eq. 22). To initialize the 15 ITD category simulations, restart files for 15-category runs are made by placing ice from each of the 5 original thickness categories from a spun up simulation into the bin of the 15 categories which includes the relevant ice thickness. This conserves sea ice volume such that the 15-category simulations are initialized with a mean thickness that is consistent with the 5-category runs. However, it does result in an initially discontinuous ITD that equilibrates over the spin-up period. Increasing the number of ITD categories from 5 to 15 increases the computational time associated with the sea ice component of the model by approximately 3x. Nonetheless, the sea ice component represents a small fraction of the model run time; for example, the sea ice model runs in 3 seconds per model day with 15 ITD categories, compared to the 5.6 seconds per model day required by the atmosphere model.

The ITD is determined by calculating the fraction of ice-covered area accounted for by each thickness category in a given region. In order to compare distributions from 5 and 15 category runs, the 15 category ITD (solid yellow lines in Figure 1) is re-binned into 5 categories with approximately the same bounds as the control run (dashed yellow lines). We utilize the NSIDC regional mask of the Arctic Ocean and its peripheral seas to delineate the results by region. Hemispheric and regional totals of sea ice area and sea ice volume are calculated using the standard method as the modeled sea ice concentration multiplied by grid cell area or grid cell area and average thickness, respectively, summed over all cells.

2.3 Observations of Arctic ITD from ICESat-2

The high-resolution freeboard measurements produced from the ATLAS laser altimeter onboard the ICESat-2 satellite launched in 2018 provide a unique opportunity to compare observations of ice thickness distribution with model outputs. Here, we use the ICESat-2 along-track sea ice thickness data (IS2SITDAT4) available through the National Snow and Ice Data Center (NSIDC, https://nsidc.org/data/is2sitdat4; Petty, Kurtz, et al., 2022). Briefly, these thickness estimates utilize high-resolution freeboard data (ATL10) provided by ICESat-2 along the three strong beams. The ATL10 freeboard data are the end result of a series of algorithms that aggregate raw photon data collected by ATLAS into sea ice height and then freeboard segments with horizontal resolutions of tens of meters and vertical uncertainties of centimeters (Kwok et al., 2021). To produce estimates of sea ice thickness, Petty et al. (2020) converted ATL10 to thickness using the hydrostatic equilibrium equation and input assumptions regarding sea ice density, snow depth, and snow density. Snow depth and density are derived from the NASA Eulerian Snow on Sea Ice Model (NESOSIM), which is a snow budget model configured for the Arctic Ocean using records of snowfall, wind, sea ice concentration, and ice drift. As the model produces relatively coarse resolution snow data ($\sim$100 km), relationships of snow depth and freeboard obtained from NASA's Operation IceBridge are used to redistribute snow onto the higher resolution ($\sim$30 m) ICESat-2 data. A more detailed description of the thickness data processing is provided in Petty et al. (2020), while recent upgrades to this

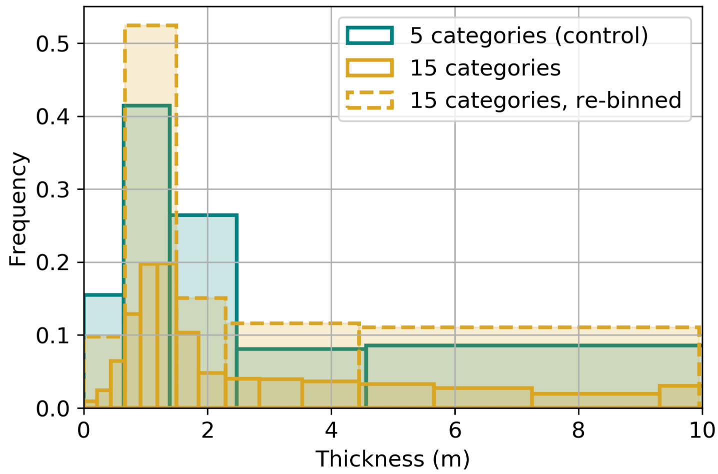

Figure 1. Example of discretized ice thickness distribution (ITD) in CICE with 5 categories (green) and 15 categories (gold, solid lines), where bars denote the frequency or fraction of ice in each ice thickness category. The 15 category ITD (gold, solid lines) can be re-binned into 5 categories with approximately the same bounds as the control (gold, dashed lines) for easier comparison.

data utilizing the latest rel005 ATL10 freeboards and NESOSIM v1.1 snow loading from November 2018 to April 2021 are presented in Petty, Keeney, et al. (2022). In this study, we use the IS2SITDAT4 thickness data from all three strong beams from November 2018 to April 2021. These data are used to calculate an ITD for a given month and region by collating all available ice thickness values within that region, and binning the data using the category bounds defined by CESM2. Thickness data are available in winter only due to availability of NESOSIM snow loading estimates. The thickness data are examined at regional scales in order to minimize any biases relating to spatial sampling of the satellite path.

Due to the use of a statistical redistribution scheme and the uncertainties of the underlying Operation IceBridge snow depths, we acknowledge that the ICESat-2 thickness observations at subgrid-scales carry large uncertainties and should be treated with caution. An alternative method could be to directly compare freeboard, rather than thickness, to minimize error associated with estimates of snow in thickness retrievals. Thickness is used here due to our focus on understanding the processes influenced by the ITD.

3 Results

3.1 Impact of ITD category resolution on simulated sea ice

We first describe the impacts of ITD category resolution on simulated sea ice mean state and the differences between results in the Arctic and Antarctic under preindustrial control forcing. This comparison uses 60-year runs with the slab ocean model. Given the relatively short length of these runs, we use a long control run that has a fully-coupled ocean (Kay et al., 2022), rather than the SOM used in experiments here, to quantify the internal variability in 25-year climatological averages. We acknowledge that the internal variability may be different in SOM and fully-coupled simulations but given the limitations in available data, this provides a reasonable approximation for simulation com-

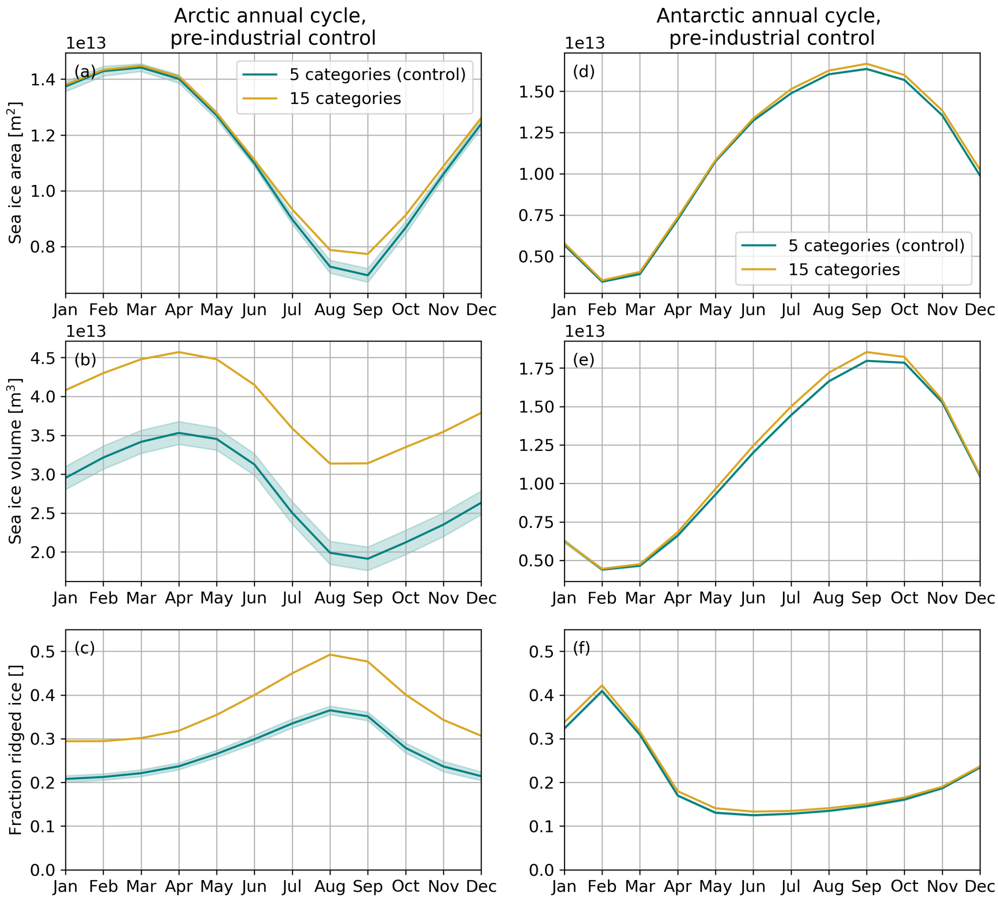

Figure 2. Mean seasonal cycle of (a-c) Arctic and (d-f) Antarctic sea ice. (a,d) Sea ice area, (b,e) volume, and (c,f) fraction of ridged ice are shown for runs with 5 categories (control; green) and 15 categories (gold). Shading represents the approximate internal variability as estimated by the standard deviation of 25-year segments of a fully-coupled preindustrial control run.

parison. The approximate internal variability as determined by the standard deviation of five randomly selected 25-year segments is shown as shading in Fig. 2.

In the Arctic, increasing the ITD category resolution in a preindustrial control climate from 5 to 15 categories results in thicker and more expansive sea ice (Fig. 2a-c). The Arctic sea ice area is approximately unchanged in the winter, but up to 30% greater at the summer sea ice minimum in September. More notably, the sea ice volume is higher year-round, indicative of thicker ice on average. There is approximately a 50% increase in volume of simulated ice at the September minimum, or about 12,268 km^3 more ice. The fraction of ridged ice is similarly about 50% greater in the winter, and around 0.1 higher year-round.

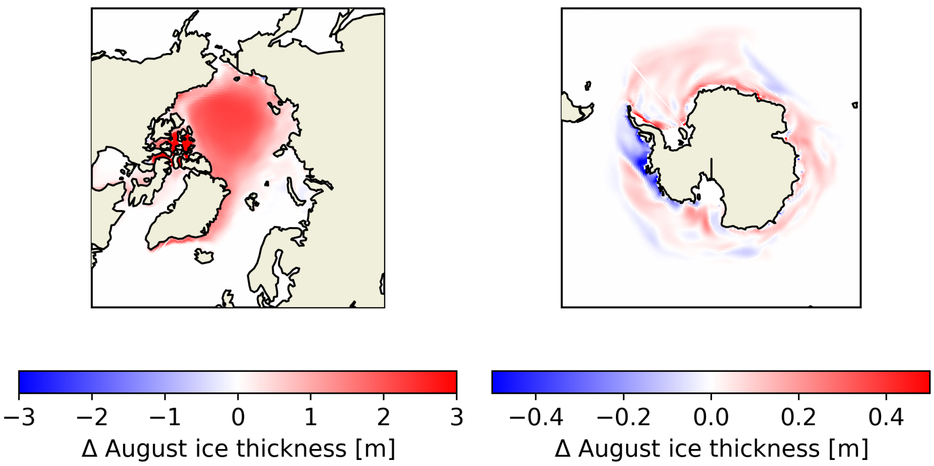

Figure 3. Difference in grid-averaged August sea ice thickness in the Arctic (left) and Antarctic (right) between run with 15 categories and 5 categories. Red indicates an increase in ice thickness with higher ITD category resolution, and blue indicates a decrease in ice thickness. Note that the scale of colorbar changes between panels.

In contrast, the mean state of Antarctic sea ice in a preindustrial control climate shows only a weak response to our ITD category resolution change (Fig. 2d-f). Both the sea ice area and sea ice volume response are somewhat larger with increased ITD category resolution in the austral winter, but approximately unchanged in the summer. The increased resolution results in a 570 km^3 increase in simulated sea ice volume at the time of maximum difference, in September. The fraction of ridged ice similarly increases a small amount, and is only significantly different from the control in winter. Though small, these differences are outside the estimated range of internal variability (shading in Fig. 2). Thus, the season of largest impact is the opposite of that in the Arctic, where summer changes were more dramatic.

Figure 3 shows the spatial distribution of changes in sea ice thickness for both hemispheres in August, which is around the time of the greatest change in each. Maps of spatial changes in sea ice thickness in February can be found in the Supporting Information (Fig. S1). In the Arctic, the map shows uniform increase in August ice thickness with higher ITD category resolution, with no areas showing a decrease in sea ice thickness. The increase in thickness is particularly high in the Canadian Islands (>3 m) but is substantial across the Central Arctic and through most of the Arctic Basin. The Antarctic has more spatial variability in average sea ice thickness change. In most regions of the Antarctic, August sea ice thickness is an average of 0–0.3 m greater. Decreases in sea ice thickness are observed primarily in the Bellinghausen and Amundsen Seas (west of the Antarctic Peninsula). This simulated decrease is primarily dynamically driven, and within the relatively high standard deviation of sea ice thickness in the control run for this region. This variability is likely related to the influence of the Southern Annular Mode (Landrum et al., 2012; Holland et al., 2017), and does not likely suggest a significant change associated with the increased ITD category resolution in the simulation.

Contributions of individual terms to the annual sea ice volume budget are examined in Figure 4. The volume changes associated with thermodynamic processes of bottom growth and top melt both decrease in the Arctic with higher ITD category resolution. In contrast, the volume of bottom growth and basal melt increase in the Antarc-

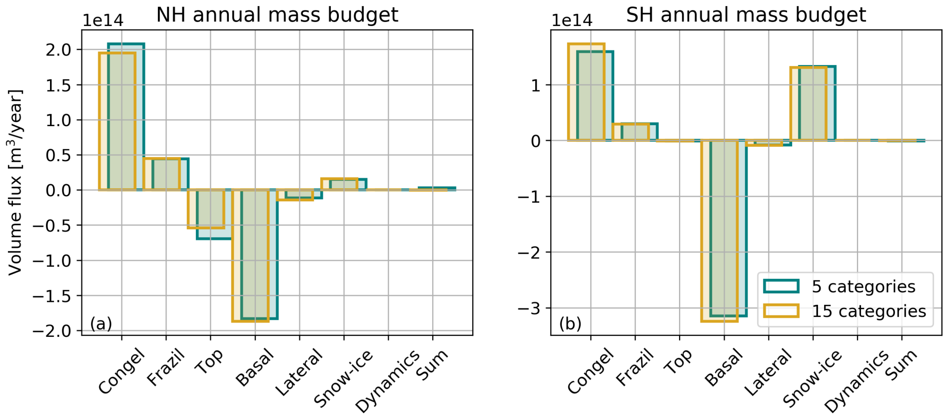

Figure 4. Annual sea ice volume budgets for preindustrial control run with 5 categories (green) and 15 categories (gold) in the (a) Arctic and (b) Antarctic. Volume budgets can be converted into mass budgets using the assumed constant sea ice density of 917 kg m^{-3} used in the model. Bars intentionally offset for visual clarity.

tic. All other terms remain approximately unchanged. Note that for hemispheric totals, the dynamics term, including ridging and advection, is by definition negligible, as it redistributes ice rather than accounting for net formation or loss. The interaction between dynamic and thermodynamic terms are discussed further in Section 3.2.

To better understand the response of the subgrid-scale ITD associated with the significant changes in Arctic sea ice thickness and volume, we examine the changes in the Central Arctic ITD and volume budget. The annual cycle of the ITD (Figure 5) shows relatively minor changes in the first two ice thickness categories with increased ITD category resolution. There is a somewhat lower fraction of open water in the summer, in agreement with the slight overall decrease in sea ice area seasonally (Fig. 2a). However, the more notable changes are in the middle and thickest ice thickness categories (1.39–2.47 m and 4.57+, respectively). There is a substantial reduction of the fraction of ice in the middle ice thickness category, which seems to be nearly completely accounted for by an increase in the thickest category. This appears to be consistent with an increase in the fraction of ridged ice in the Arctic by about 0.1 throughout the year (Fig. 2c). It is possible that more of the thinner ice is ridged, rather than being promoted by ice growth to the mid-range ice category (1.39-2.47 m), or that more of the 1.39-2.47 m ice specifically is ridged, moving it into the thickest ice category. As the fraction of ridged ice is not tracked as a function of ice thickness category in these runs, it is not possible to confirm this more specifically from the model outputs.

Comparison of the volume budgets for the Central Arctic (Fig. 6) shows the changes in thermodynamic and dynamic processes associated with the higher resolution and shift in sea ice mean state. As with the Arctic hemispheric totals (Fig. 4), we see a decrease in thermodynamic terms of bottom growth, and surface and basal melt. This is likely associated with the decrease in the fraction of thin categories (Fig. 5), as thin ice typically undergoes more rapid growth and melt. The role of thermodynamic processes decreases with higher ITD category resolution due to the shift of the mean state towards the thickest ice category because of the weaker simulated strength driving more active ridging. The increase in ice volume loss due to dynamics suggests an increase in advection of ice out of the region, as ridging conserves ice volume locally.

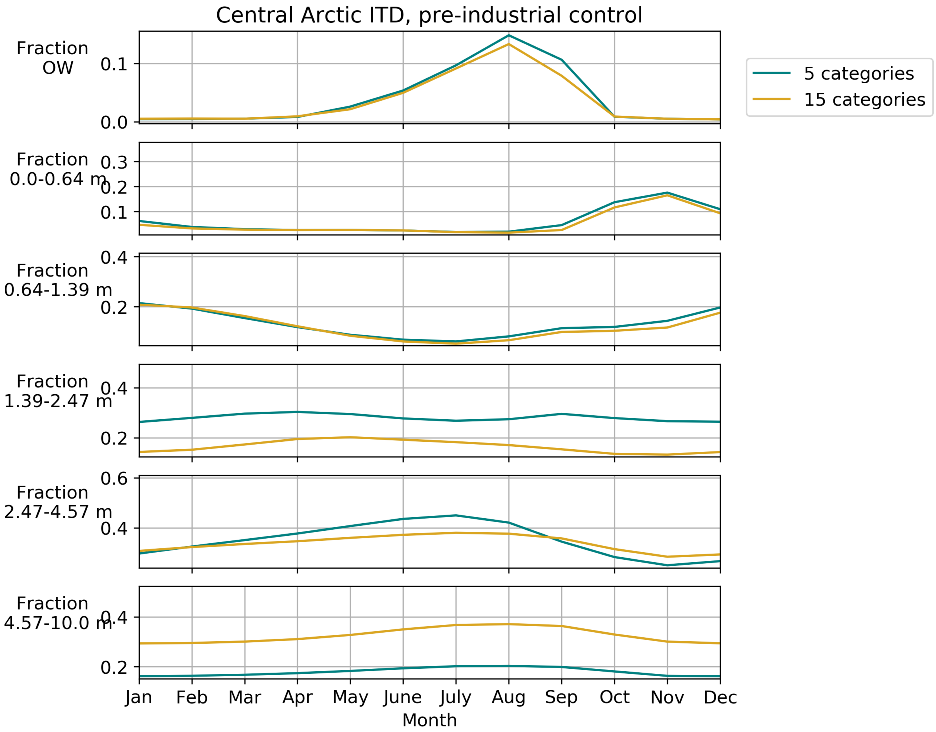

Figure 5. Mean annual cycle of ice thickness distribution in the Central Arctic (as defined by NSIDC), preindustrial forcing. The fractional coverage of open water and each ice category is shown for the control run (green) and 15 category run (gold). As in Fig. 1, 15 categories are re-binned into 5 categories with approximately the same bounds as the control.

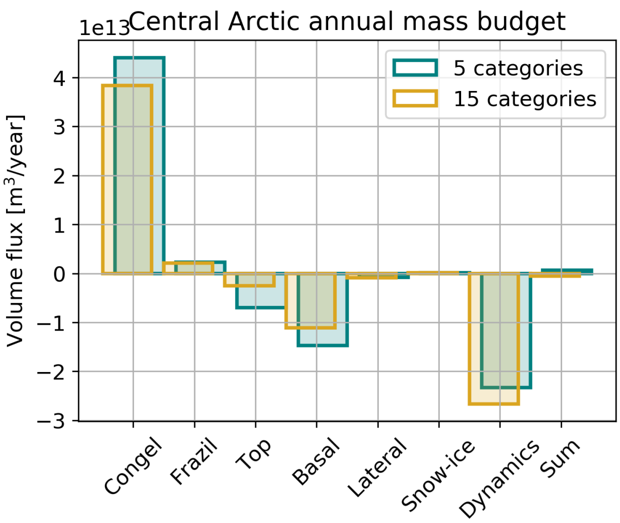

Figure 6. Annual sea ice volume budget for the Central Arctic in preindustrial control run with 5 categories (green) and 15 categories (gold). Volume budgets can be converted into mass budgets using the assumed constant sea ice density of 917 kg m^{-3} used in the model.

3.2 Causes of ITD-related differences in sea ice simulation

We next examine the primary causes behind the differences in simulated sea ice with 15 ITD categories. In particular, we compare the differences between the two hemispheres, and examine the primary dynamic and thermodynamic processes responsible for the observed changes.

To understand the role of sea ice dynamics in changes in simulated sea ice thickness, we first investigate the changes in simulated ice strength. In CESM2, ice strength is calculated for each grid-cell and depends on the ITD, as described in Section 2.1. In general, a lower mean thickness will result in weaker ice (Fig. 7). Compressive deformation of the ice increases with lower strength such that the fraction of ice that is ridged increases with weaker ice. Figure 7 shows that, for the same mean grid-cell sea ice thickness, increased ITD category resolution in the Arctic results in generally weaker ice. This is particularly true for grid cells with mean thickness of 5 m or greater. These results are consistent with the seasonal cycle of the ITD in the Central Arctic (Figure 5) suggesting that increasing the resolution of the ITD primarily impacts relatively thick ice categories in the Arctic. Figure 7 shows results for December, but the result is consistent with other winter months. In effect, higher ITD category resolution of thick ice leads to weaker ice which undergoes more dynamic ridging. In particular, the model suggests a $\sim$50% increase in the fraction of Arctic winter ice that is in the thick ridged ice category, from 0.2 to 0.3 (Fig. 2c). The fraction of ridged ice is generally higher in the Arctic summer due to the preferential melt of thin ice. The fraction of ridged ice reaches 0.49 in August with 15 ITD categories, compared to 0.36 in the 5 ITD category run (Fig. 2c). Notably, increased ITD category resolution is not associated with the same increase in average strength in the Antarctic (Fig. 7). The Antarctic ice pack has less persistent ridged ice and an overall thinner ice pack (Fig. 2e-f), resulting in less of the especially thick ($>$ 5 m) ice where the effect of resolution was particularly notable for sea ice strength in the Arctic.

To isolate the impact of ITD category resolution on thermodynamic processes, we examine the changes in simulated bottom growth rates. We acknowledge that, in comparison to strength, thermodynamic mass budget terms can vary spatially due to the relationship with the heat budget, which could impact these comparisons. While the spatial distribution of sea ice is relatively unchanged in the Antarctic, spatial changes in sea ice thickness in the Arctic (Fig. 3) are more substantial. In both the Arctic and Antarctic, the bottom growth rate peaks around 0.5–1.0 m mean thickness (Fig. 8). Ice less than 0.5 m thickness is more likely to be near the ice edge where the atmosphere is warmer and growth rates are slower. The average bottom growth rate in the Arctic is largely unchanged by the increase in ITD category resolution (with similar patterns seen in the analysis of the Central Arctic, suggesting a small role of spatial redistribution). There is more bottom growth in Antarctic sea ice for grid cells of the same mean sea ice thickness between 0.5–2.5 m (Fig. 8). Results are shown for June, but a similar direction and magnitude of change is seen for all winter months. The impact is particularly clear for relatively thin ice, around 0.5-1.5 m thick. Thermodynamic growth is non-linear with ice thickness, and tends to be more rapid for thinner ice as it allows for more heat conduction from the ice-ocean interface. For the same average thickness, more ITD categories will allow better resolution of thin ice categories. As a result, the increase in bottom growth throughout the growth season is associated with an increase in sea ice thickness across much of the Antarctic sea ice pack (Fig. 8). Mass budget analysis (Fig. 4) shows that increase in bottom growth is offset by similar increase in the rate of basal melt, such that the ice volume and area return to the levels of the control run in the spring and summer (Fig. 2d,e).

While the results in Figure 8 suggest that thermodynamic processes in the Arctic are not significantly impacted directly by the higher resolution of the ITD, changes in the sea ice volume budgets in Figures 4 and 6 demonstrate the interaction between

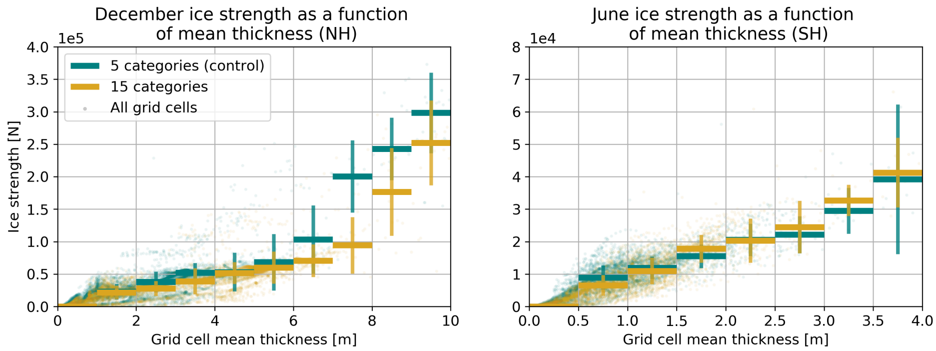

Figure 7. Sea ice strength as a function of grid-cell mean sea ice thickness in December (Arctic; left) and June (Antarctic; right). Runs with 5 categories (control; green) and 15 categories (gold). Transparent circles show points from all grid cells in all analyzed years, with solid bars showing binned means with length indicating standard deviation.

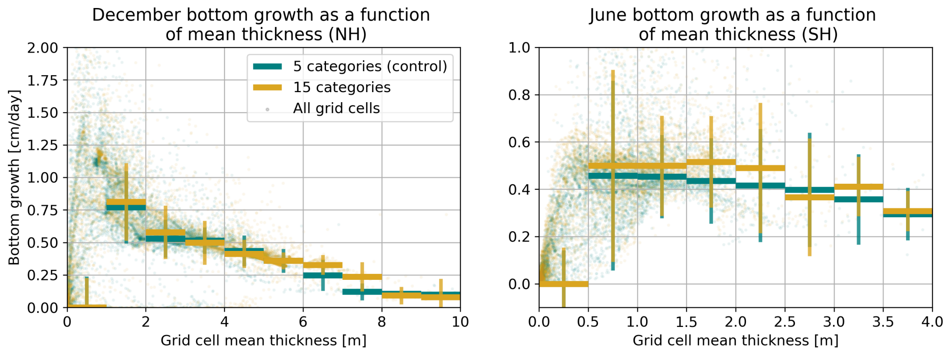

Figure 8. Bottom growth rate as a function of sea ice thickness for December (Arctic; left) and June (Antarctic; right). Runs with 5 categories (control; green) and 15 categories (gold). Transparent circles show points from all grid cells in all analyzed years, with solid bars showing binned means with horizontal length indicating standard deviation.

the thermodynamic and dynamic processes presented here. The increase of ridging brings the sea ice to a new equilibrium ice thickness (Fig. 2; C. Bitz & Roe, 2004) such that the ice growth equals ice melt. We may be more likely to see a relative increase in growth associated with ridging (which conserves volume) in the transient response. As we can see in Figure 8, the rate of growth is not equal across average thickness. Dynamics (ridging) is moving ice into thicker categories where bottom growth and surface melt are weaker. In other words, decreases in thermodynamic processes are not a direct impact of the resolution of categories as it relates to growth or melt, but rather appear to be an indirect result of subgrid-scale thickness redistribution due to ridging.

3.3 Comparison with ICESat-2 thickness estimates

High spatial resolution estimates of sea ice thickness derived from ICESat-2 freeboard data provide a unique opportunity to assess the modeled ITDs. We do not expect the model to precisely capture ITDs derived from ICESat-2 data, as there are many factors in addition to the ITD category resolution that impact this comparison. This includes that the model is not using an exact forcing from reanalysis, but rather represents similar climatological conditions to what we would expect over the observed time period. Additionally, the ICESat-2 thickness estimates rely on snow loading from a relatively simple snow accumulation model framework and empirical assumptions regarding small-scale snow distribution. Thickness retrievals may be particularly problematic in areas of relatively high snowfall and low freeboard (such as can occur in the Barents Sea) and areas of heavily ridged ice. Nonetheless, comparisons between observations and models are useful for understanding process differences across regions and how they may be represented in our current models and observational datasets.

For model comparisons, we use outputs from the SSP-3.70 scenario simulation (Kay et al., 2022), which begins in 2015. Averages from 2015-2025 are used to center on the time covered by observations, and the simulated sea ice is shown in Figure 9. The impact of increasing ITD category resolution is less dramatic than in preindustrial control runs, similarly resulting in a substantial increase in sea ice volume year-round and a greater fraction of ridged ice, but with no change in the sea ice area (Fig. 9). These runs use tuned albedo characteristics that improve the simulation of the sea ice state over the historical period (Kay et al., 2022), and by extension, we expect that the Arctic sea ice over this period in the control run is appropriate for the climate state. We use the four available SSP3-7.0 ensemble members (Kay et al., 2022) to estimate the associated internal variability. The standard deviation of the annual cycle for the 10-year interval is shown as shading around the mean in Figure 9. As the changes noted are outside the range of internal variability, subsequent analysis will proceed with one ensemble member.

We present comparisons of the ITD from the Central Arctic and Barents Sea to highlight processes in regions dominated by perennial and seasonal ice regimes, respectively. While ICESat-2 will not provide full coverage over each region for any given month due to the satellite orbit cycle, combining all observations for a given month results in a sufficient number of observations such that we can expect it to be statistically representative. For example, the Central Arctic has an average of 1.7×10^9 ICESat-2 thickness observations for each month across all months and years, with a monthly minimum of 8.7×10^8 during one month. The Barents Sea has an average of 5.2×10^7 ICESat-2 thickness observations for each month across all months and years, with a monthly minimum of 2.4×10^5 during a month with particularly low returns. Figures for results of all other Arctic Basin regions are included in the Supporting Information. ICESat-2 observes sea ice freeboard in both hemispheres, but we only show comparisons in the Arctic here as thickness estimates are not available for the Antarctic due to the added complexity of modeling snow on Southern Hemisphere sea ice.

Comparisons of ITD are displayed in two ways to highlight different aspects. Plots of the mean annual cycle (Figures 10 and 12) highlight the seasonal changes, where we can compare quantities within individual categories. Here, the fraction in each category is scaled by the total ice concentration such that the values represent the fraction of the entire region covered by ice in that thickness range. As each category has an associated average thickness within the bounds, changes in fractions do not capture all changes in the mean thickness. Growth and melt do not necessarily transfer ice to new categories depending on the average thickness, but typically will on monthly time scales. As regional ice concentration estimates are not directly available from the ICESat-2 thickness data, the observational ITD are scaled by the ice concentration in the 5 category run. These plots also highlight estimates of interannual variability, where the total range of values over the 10 analyzed years of the model and 3 years of ICESat-2 are represented by the shaded areas, and the solid line represents the mean in both datasets. The differences noted here are generally outside the range of inter-annual variability. Histograms from selected months (Figures 11 and 13) show the absolute value of fractions in ice-covered areas. We note again that the re-binning of the 15 category run results in slightly different bin edges than in the 5 category run (Fig. 1), but we expect this to have a negligible impact on the comparison.

In almost all regions, the model in both resolutions predicts significantly more ice in the thickest ice category than the ICESat-2 observations (e.g., Figs. 10 and 12). Higher

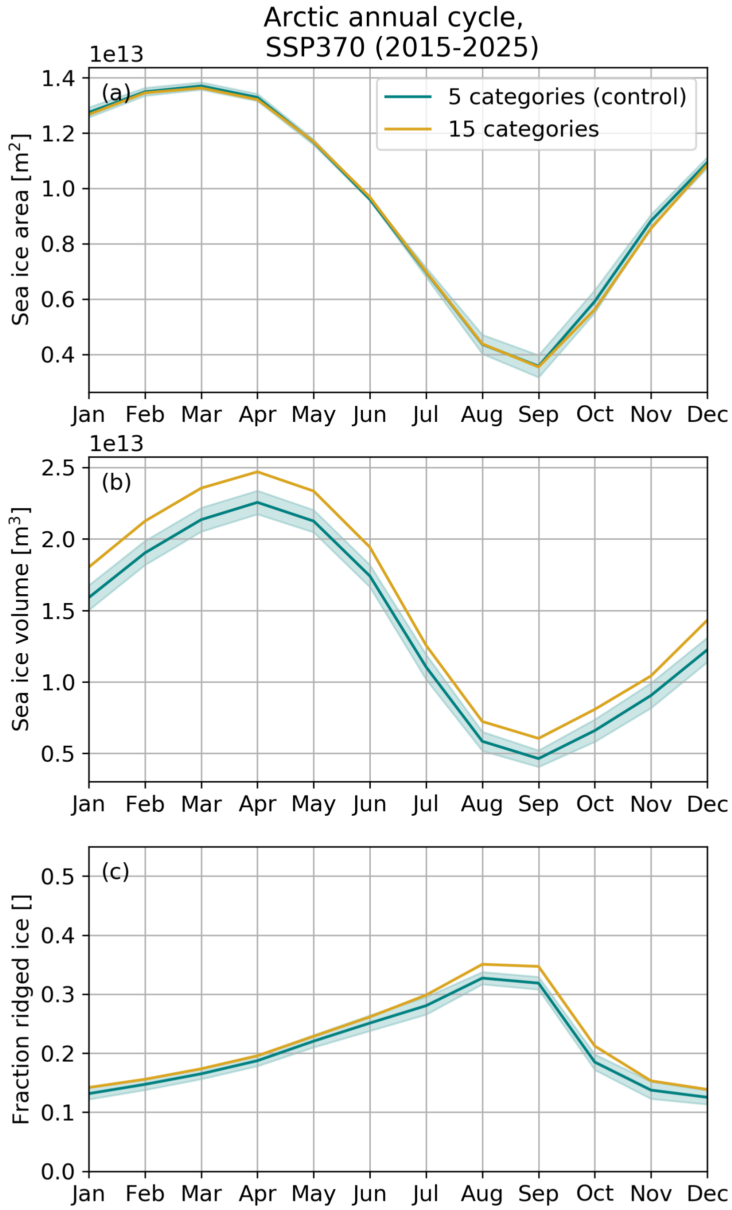

Figure 9. Simulated seasonal cycle of Arctic (a) sea ice area, (b) volume, and (c) ridged ice fraction, over years 2015-2025 (SSP3-7.0). Runs with 5 categories (control; green), where shading represents the approximate internal variability as estimated by the standard deviation around the ensemble mean using four ensemble members (Kay et al., 2022), and 15 categories (gold).

resolution of ITD results in an even higher fraction of ice in the thickest category (4.57+ m) compared to the control, and thus is even further from the estimate from observations. Ice of such thickness can only be achieved by ridging. The observed seasonal cycle of thick, ridged ice in the Central Arctic has a strong amplitude, where there is almost no ice in the thickest category at the start of fall freeze-up and the fraction rapidly increases through the fall and winter (Fig. 10). In comparison, the modeled ice in the thickest category is persistent through the summer, but is comparable to observations by April. The seasonal changes in thick ice warrant further exploration in future work, in particular to understand the potential impact of the preferential melt of thick, ridged ice over the summer (e.g., Wadhams, 2000; Schramm et al., 2000). We note that while it is possible that the ability of ICESat-2 to resolve the range of thicknesses impacts the comparison, recent work has suggested that ICESat-2 can resolve small-scale freeboard variability, including leads and pressure ridges, with centimeter-scale accuracy (Kwok et al., 2019; Farrell et al., 2020). The snow model, NESOSIM, used to convert freeboard to thickness, has been calibrated using recent snow depths obtained from NASA's Operation IceBridge at regional-scales in the most recent release used here (Version 1.1; Petty, Keeney, et al., 2022). However, questions still remain regarding snow distribution over ridges. The Operation IceBridge Snow Radar-derived snow depth observations used to estimate the empirical relationship between freeboard and small-scale snow depth variability are noted to be more uncertain over ridged/deformed ice regimes compared to thin level ice (King et al., 2015). If less snow is retained over ridges compared to current assumptions, this would increase the effective sea ice thickness estimates from ICESat-2 (Nicolaus et al., 2022).

The fractional coverage of thin ice categories is driven by dynamics as well as thermodynamics, as ridging can cause a loss of ice from these categories. The growth of relatively thin and new ice is well-captured by comparisons in the Barents Sea, which is predominately seasonal ice (i.e., open water fraction is nearly 1 at the September minimum; Fig. 12). Thin and new ice growth generally compares well with ICESat-2 observations. In particular, the rate of change of ice concentration in the 1st and 2nd categories in the Barents Sea (0.0–0.64 and 0.64–1.39 m) are comparable from fall through winter (Fig. 12). The model representation of the seasonal cycle of thin ice in the 5 category control run matches particularly well with observations, and the growth of new ice possibly becomes too rapid compared to observations with the increased ITD category resolution of the 15 category run. Thus, higher ITD category resolution results in a lower quality comparison with observations in regions dominated by seasonal, thin ice. The volume contribution from advection makes up substantial fraction of the Barents Sea ice volume change in the fall (≈30% in November), but is likely primarily new ice growth from neighboring regions such that we can justify treating the ITD changes as primarily thermodynamic.

Model simulations appear to estimate a lower fraction of ice in intermediate thickness categories compared to ICESat-2 observations. This is evident in the Central Arctic throughout the periods of comparison (Fig. 11), and the Barents Sea region in the fall (Fig. 13). This may be related to more thin ice being ridged in the model, rather than being promoted to thicker ice by growth processes.

4 Discussion

4.1 Implications for choice of ITD category resolution

The primary aim of this study was to assess the effect of increases in the ITD category resolution in a coupled model framework, rather than a more robust recommendation of the optimal number of thickness categories. Nonetheless, it highlights some considerations for choosing model setup. Increasing the ITD category resolution currently results in increased disagreement with ICESat-2-derived thickness estimates for most thick-

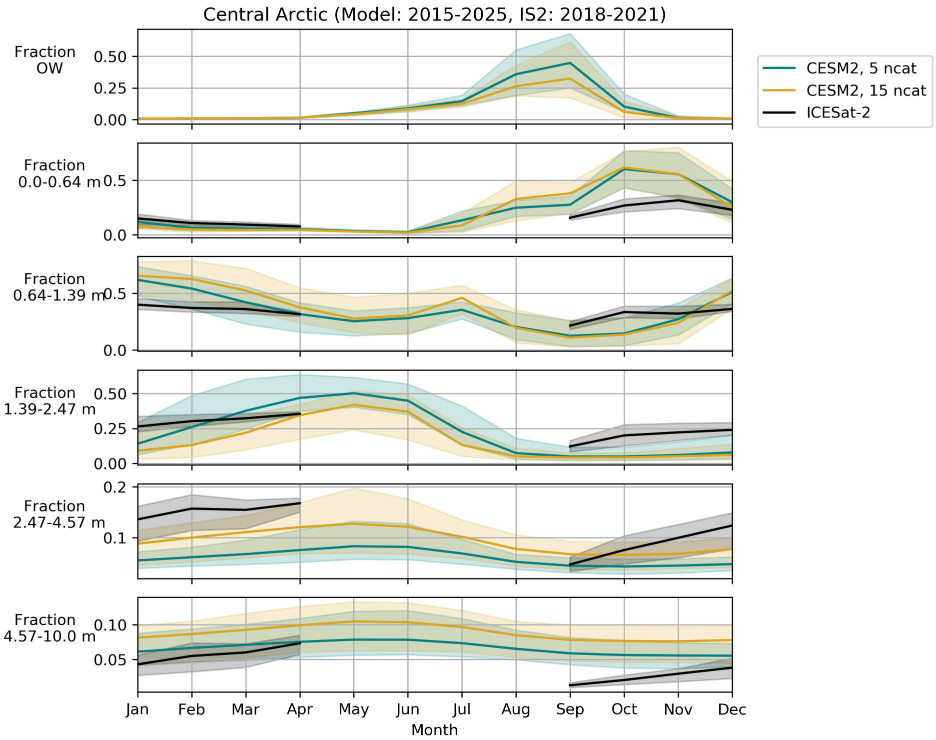

Figure 10. Mean annual cycle of the ice thickness distribution in the Central Arctic in model simulations and ICESat-2 observations. The fractional coverage of open water and in each ice category is shown for the control 5 category model run (green), 15 category model run (gold), and ICESat-2 (black). Shading represents the full range of values over the 10 years analyzed from the model or the 3 years of observations.

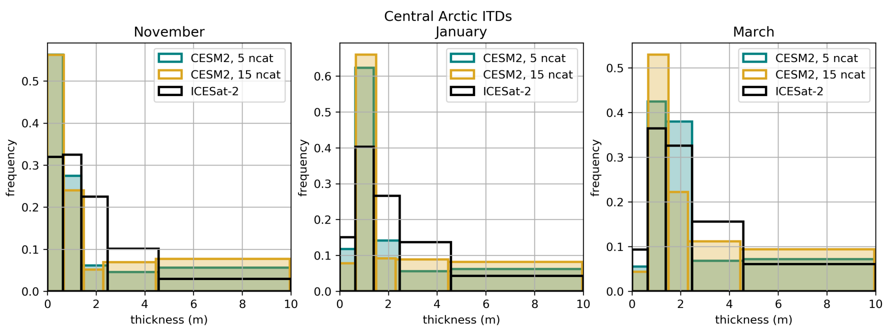

Figure 11. Comparison of discretized ice thickness distribution in the Central Arctic in model simulations and ICESat-2 for select months: November, January, and March. The average fraction of ice coverage in each category is shown for the 5 category model run (green), 15 category model run (gold), and ICESat-2 (black outline).

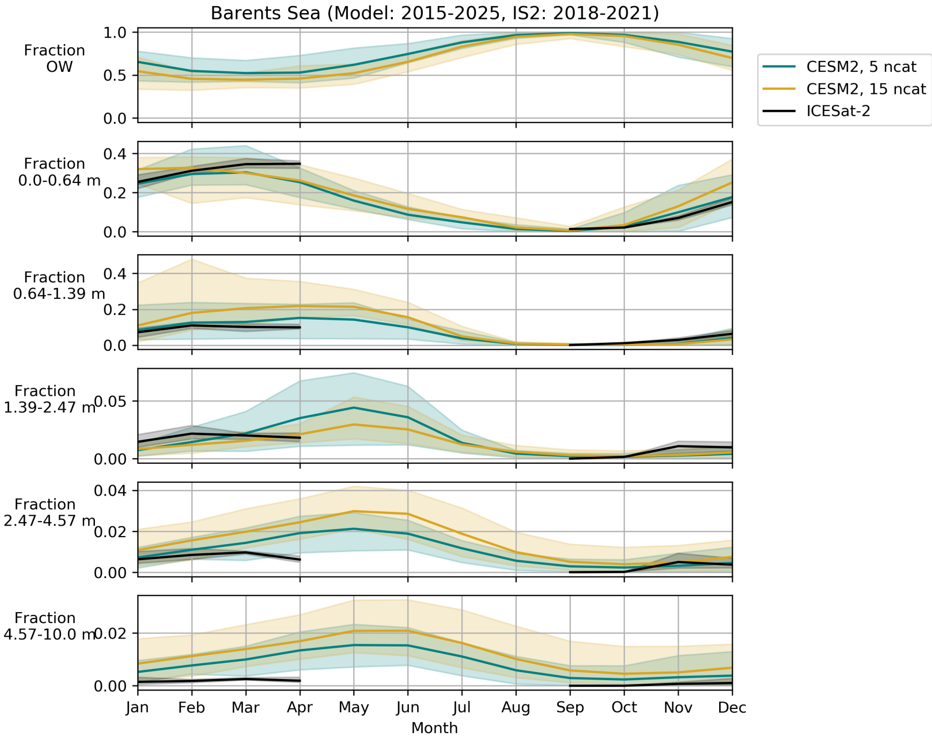

Figure 12. Mean annual cycle of the ice thickness distribution in the Barents Sea in model simulations and ICESat-2 observations. The fractional coverage of open water and in each ice category is shown for the control 5 category model run (green), 15 category model run (gold), and ICESat-2 (black). Shading represents the full range of values over the 10 years analyzed from the model or the 3 years of observations.

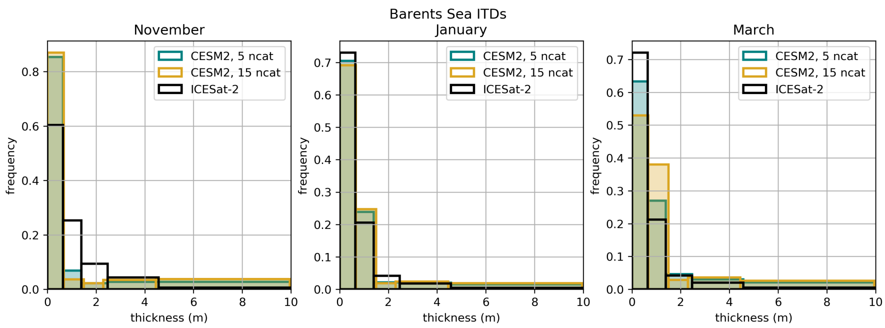

Figure 13. Comparison of discretized ice thickness distribution in the Barents Sea in model simulations and ICESat-2 for select months: November, January, and March. The average fraction of ice coverage in each category is shown for the 5 category model run (green), 15 category model run (gold), and ICESat-2 (black outline).

ness categories (Figs. 10, 12), and is particularly poor for thick categories, which has a significant impact on the sea ice mean state (Fig. 9). Tuning the model (e.g., Kay et al., 2022) or revisiting parameterizations could improve the mean state simulation and the ITD comparisons. Additionally, if completing a study focused on understanding the interactions of the sea ice with other components of the climate model, using 15 categories may provide benefits. An ITD with more categories should result in less numerical diffusion (smoothing of peaks), and result in better representation of thermodynamic growth processes and the redistribution from thin to thick ice. More ITD categories is likely especially important in climate system where multiple ice types are present (i.e., multi-year and first-year ice) such that multiple peaks can be resolved simultaneously. Studies focused on understanding evolution of sea ice processes, and in particular on investigating sea ice variability, will likely benefit from better resolution of the ITD provided by more categories (i.e. Massonnet et al., 2019). While we only completed a 15-category run here, similar directional impact can be expected from runs with increasing the number of categories to other specific values (Massonnet et al., 2019). Although it can have significant increases on the computational time associated with the sea ice component, the sea ice component remains a relatively small computational expense in the context of a fully or partially-coupled model (i.e., the slab ocean model, as used here).

Most CMIP6 global sea ice models have a known low bias in Arctic sea ice volume over the historical period (Notz & Community, 2020). In light of this, considering the role of the number of ITD categories on key sea ice processes should prove useful in targeting future improvements. For example, the standard version of the CESM2 model used here has a known thin bias in the Arctic sea ice pack (Danabasoglu et al., 2020; DeRepentigny et al., 2020). This may be related to the under-prediction of ice in the intermediate thickness categories (e.g., Fig. 11) despite the apparent over-prediction of the thickest ice category. While our results suggest that increasing the number of categories increases the simulated thickness and volume (Fig. 9b), the albedo tunings used in Kay et al. (2022) to produce a more realistic ice pack show that there are many additional factors that could be considered in relation to better thickness representation. We propose that the under-representation of ice in intermediate thickness categories in the model is at least in part a result of the propensity for ridging, which moves ice towards thicker categories. Understanding the factors contributing to disagreement in these categories should be a focus for efforts to improve model representation of ice thickness in global climate models. To do so, more effort should also be devoted to better observing and characterizing the expected ice thickness distributions at basin scales.

The realism of many thickness-dependent parameterizations, such as the sea ice strength, is largely uncertain. As such, adjustment to the number of ITD categories may be more beneficial with future changes to thickness-dependent parameterizations. The results in Section 3.3 suggest that there is even more thick, ridged ice in the model than is estimated based on satellite observations due to the dependence of the current parameterization for ice strength on ITD category resolution. Ungermann et al. (2017) similarly concluded that the strength formulation by Rothrock (1975) strongly depends on the number of ITD categories. Updated strength and ridging parameterizations are likely needed to allow improved prediction of sea ice. Thus, the ideal number of ITD categories should be re-evaluated after new parameterizations are implemented. In particular, it is possible that 5 categories may not be enough to sufficiently resolve thick ice categories with the implementation of more advanced ridging schemes (e.g., E. C. Hunke, 2014). Higher-resolution simulation of thin ice will additionally affect the sea ice growth rates, with implications for the ice-ocean coupling. The formation of open water is also related to the resolution of the thinnest ice categories, so melting is similarly expected to be dependent on the number of ITD categories, especially with implementation of more advanced lateral melting and floe size distribution schemes (e.g., Roach et al., 2018; Smith et al., 2022).

5 Conclusions

This study suggests that the resolution of the sea ice thickness distribution (ITD) has a substantial impact on sea ice processes in a coupled climate model. Sensitivity analysis of runs with an increased number of ITD categories in a control climate suggest the following key points:

- Increasing the ITD category resolution in the coupled model significantly increases the simulated Arctic sea ice thickness and is primarily dynamically-driven, while increases in Antarctic sea ice are relatively minor and primarily thermodynamically-driven.
- Dynamic impacts of increasing ITD category resolution primarily moves ice from thinner to thicker ice categories due to the thickness-dependent representation of ice strength, which results in weaker ice and more ridging. Dynamic impacts are especially noticeable in the Arctic summer ice pack when proportions of ridged ice remain high.
- Thermodynamic impacts of increasing ITD category resolution result in both more melt and growth across ice thicknesses in the Antarctic winter ice pack due to the larger impact on growth via the ice thickness-ice growth rate feedback. (C. Bitz & Roe, 2004).

These results are consistent with previous work indicating that thinnest categories are most sensitive to thermodynamic processes, while thickest categories are most sensitive to dynamic processes (Moreno-Chamarro et al., 2020; E. C. Hunke, 2014). We expect the dynamic impact of higher ITD category resolution to decrease over time as Arctic sea ice becomes thinner and less ridged on average, as demonstrated by the results of the future scenario SSP3-7.0.

In addition, this study provides the first comparisons of estimates of subgrid-scale ITD from high-resolution ICESat-2 freeboard observations and state-of-the-art coupled sea ice model output. Comparisons of model outputs with satellite-derived data suggest targets for future work:

- Improvements in simulating Arctic sea ice thickness should focus on ice strength and ridging parameterizations. A number of recent efforts have been focusing on improved ridging schemes (e.g., Roberts et al., 2019) which could be tested and incorporated into coupled models.
- Ice thickness distribution provides an under-utilized opportunity for insights into sea ice schemes in coupled climate models, beyond mean state and grid-cell average thickness.
- The optimum number of ITD categories should be revisited depending on the application, but tuning will likely be required as many current settings have been determined based on the default resolution of five categories.
- The ICESat-2-derived thickness estimates rely on modelled estimates of small-scale snow redistribution that needs to be better informed by the latest in observational data towards achieving more reliable ice thickness estimation.

Acknowledgments

The CESM project is supported primarily by the National Science Foundation. Computing and data storage resources, including the Cheyenne supercomputer (https:// doi.org/10.5065/ D6RX99HX), were provided by the Computational and Information Systems Laboratory (CISL) at NCAR. We thank all the scientists, software engineers, and administrators who contributed to the development of CESM2. Thank you to Bill Lipscomb for helpful conversations relating to the ITD. The ICESat-2 along-track Arctic sea ice thickness estimates are publicly available through the NSIDC (IS2SITDAT4 Version 1, https://nsidc.org/data/is2sitdat4).

MMS was supported by NSF OPP-1724467 and OPP-1724748 and OPP-2138787. MMH was supported by NSF OPP-1724748. BL was supported by NSF OPP-1724467 and OPP-2138787. DAB was supported by NCAR, which is a major facility sponsored by the NSF under Cooperative Agreement No. 1852977. AAP was supported by the ICESat-2 Project Science Office.

References

Bacmeister, J., Hannay, C., Medeiros, B., Gettelman, A., Neale, R., Fredriksen, H., ... others (2020). Co 2 increase experiments using the cesm: Relationship to climate sensitivity and comparison of cesm1 to cesm2. *Journal of Advances in Modeling Earth Systems*, *12*(11), e2020MS002120.

Bailey, D. A., Holland, M. M., DuVivier, A. K., Hunke, E. C., & Turner, A. K. (2020). Impact of a new sea ice thermodynamic formulation in the cesm2 sea ice component. *Journal of Advances in Modeling Earth Systems*, *12*(11), e2020MS002154.

Bitz, C., & Roe, G. (2004). A mechanism for the high rate of sea ice thinning in the arctic ocean. *Journal of Climate*, *17*(18), 3623–3632.

Bitz, C. M., Holland, M. M., Weaver, A., & Eby, M. (2001). Simulating the ice-thickness distribution in a coupled climate model. *Journal of Geophysical Research: Oceans*, *106*(C2), 2441–2463.

Bitz, C. M., Shell, K., Gent, P., Bailey, D., Danabasoglu, G., Armour, K., ... Kiehl, J. (2012). Climate sensitivity of the community climate system model, version 4. *Journal of Climate*, *25*(9), 3053–3070.

Danabasoglu, G., Lamarque, J.-F., Bacmeister, J., Bailey, D., DuVivier, A., Edwards, J., ... others (2020). The community earth system model version 2 (cesm2). *Journal of Advances in Modeling Earth Systems*, *12*(2), e2019MS001916.

DeRepentigny, P., Jahn, A., Holland, M. M., & Smith, A. (2020). Arctic sea ice in two configurations of the cesm2 during the 20th and 21st centuries. *Journal of Geophysical Research: Oceans*, *125*(9), e2020JC016133.

Farrell, S., Duncan, K., Buckley, E., Richter-Menge, J., & Li, R. (2020). Mapping sea ice surface topography in high fidelity with icesat-2. *Geophysical Research Letters*, *47*(21), e2020GL090708.

Flato, G. M., & Hibler III, W. D. (1995). Ridging and strength in modeling the thickness distribution of arctic sea ice. *Journal of Geophysical Research: Oceans*, *100*(C9), 18611–18626.

Hibler, W. D. (1979). A dynamic thermodynamic sea ice model. *Journal of physical oceanography*, *9*(4), 815–846.

Holland, M. M., Bitz, C. M., Hunke, E. C., Lipscomb, W. H., & Schramm, J. L. (2006). Influence of the sea ice thickness distribution on polar climate in ccsm3. *Journal of Climate*, *19*(11), 2398–2414.

Holland, M. M., Bitz, C. M., & Weaver, A. (2001). The influence of sea ice physics on simulations of climate change. *Journal of Geophysical Research: Oceans*, *106*(C9), 19639–19655.

Holland, M. M., & Curry, J. A. (1999). The role of physical processes in determining the interdecadal variability of central arctic sea ice. *Journal of climate*, *12*(11), 3319–3330.

Holland, M. M., Landrum, L., Kostov, Y., & Marshall, J. (2017). Sensitivity of antarctic sea ice to the southern annular mode in coupled climate models. *Climate Dynamics*, *49*(5), 1813–1831.

Hunke, E., Lipscomb, W., Jones, P., Turner, A., Jeffery, N., & Elliott, S. (2017). *Cice, the los alamos sea ice model* (Tech. Rep.). Los Alamos National Lab.(LANL), Los Alamos, NM (United States).

Hunke, E. C. (2014). Sea ice volume and age: Sensitivity to physical parameterizations and thickness resolution in the cice sea ice model. *Ocean Modelling*, *82*, 45–59.

Hunke, E. C., Lipscomb, W. H., Turner, A. K., Jeffery, N., & Elliott, S. (2015). *CICE: the Los Alamos Sea Ice Model Documentation and Software User's Manual Version 5.1 LA-CC-06-012* (Tech. Rep.). Los Alamos National Laboratory. Retrieved from `http://oceans11.lanl.gov/trac/CICE`

Jahn, A., Sterling, K., Holland, M. M., Kay, J. E., Maslanik, J. A., Bitz, C. M., ... others (2012). Late-twentieth-century simulation of arctic sea ice and ocean properties in the ccsm4. *Journal of Climate*, *25*(5), 1431–1452.

Kay, J. E., DeRepentigny, P., Holland, M., Bailey, D., DuVivier, A., Blanchard-Wrigglesworth, E., ... Rosenbloom, N. (2022). Less surface sea ice melt in the cesm2 improves arctic sea ice simulation with minimal non-polar climate impacts. *Journal of Advances in Modeling Earth Systems*, doi: 10.1029/2021MS002679.

Keen, A., Blockley, E., Bailey, D., Boldingh Debernard, J., Bushuk, M., Delhaye, S., ... others (2021). An inter-comparison of the mass budget of the arctic sea ice in cmip6 models. *The Cryosphere*, *15*(2), 951-982.

King, J., Howell, S., Derksen, C., Rutter, N., Toose, P., Beckers, J. F., ... Richter-Menge, J. (2015). Evaluation of operation icebridge quick-look snow depth estimates on sea ice. *Geophysical Research Letters*, *42*(21), 9302–9310.

Kwok, R., Kacimi, S., Markus, T., Kurtz, N., Studinger, M., Sonntag, J., ... Harbeck, J. (2019). Icesat-2 surface height and sea ice freeboard assessed with atm lidar acquisitions from operation icebridge. *Geophysical Research Letters*, *46*(20), 11228–11236.

Kwok, R., Petty, A., Wimert, J., Bagnardi, M., Cuningham, G., Hancock, D., ... Kurtz, N. (2021). *Ice, cloud, and land elevation satellite-2 project: Algorithm theoretical basis document (atbd) for sea ice products* (Tech. Rep. No. Release 005). Ice, Cloud, and Land Elevation Satellite-2 Project: Algorithm Theoretical Basis Document (ATBD) for Sea Ice Products, Release 005.

Landrum, L., Holland, M. M., Schneider, D. P., & Hunke, E. (2012). Antarctic sea ice climatology, variability, and late twentieth-century change in ccsm4. *Journal of Climate*, *25*(14), 4817–4838.

Lipscomb, W. H. (2001). Remapping the thickness distribution in sea ice models. *Journal of Geophysical Research: Oceans*, *106*(C7), 13989–14000.

Massonnet, F., Barthélemy, A., Worou, K., Fichefet, T., Vancoppenolle, M., Rousset, C., & Moreno-Chamarro, E. (2019). On the discretization of the ice thickness distribution in the nemo3. 6-lim3 global ocean–sea ice model. *Geoscientific Model Development*, *12*(8), 3745–3758.

Massonnet, F., Fichefet, T., Goosse, H., Vancoppenolle, M., Mathiot, P., & König Beatty, C. (2011). On the influence of model physics on simulations of arctic and antarctic sea ice. *The Cryosphere*, *5*(3), 687–699.

Massonnet, F., Vancoppenolle, M., Goosse, H., Docquier, D., Fichefet, T., & Blanchard-Wrigglesworth, E. (2018). Arctic sea-ice change tied to its mean state through thermodynamic processes. *Nature Climate Change*, *8*(7), 599–603.

Maykut, G. A. (1982). Large-scale heat exchange and ice production in the central arctic. *Journal of Geophysical Research: Oceans*, *87*(C10), 7971–7984.

Moreno-Chamarro, E., Ortega, P., & Massonnet, F. (2020). Impact of the ice thickness distribution discretization on the sea ice concentration variability in the nemo3. 6–lim3 global ocean–sea ice model. *Geoscientific Model Development*, *13*(10), 4773–4787.

Nicolaus, M., Perovich, D. K., Spreen, G., Granskog, M. A., von Albedyll, L., Angelopoulos, M., ... Wendisch, M. (2022). Overview of the mosaic expedition - snow and sea ice. *Elementa Science of the Anthropocene*, https://doi.org/10.1525/elementa.2021.000046.

Notz, D., & Community, S. (2020). Arctic sea ice in cmip6. *Geophysical Research Letters*, *47*(10), e2019GL086749.

Petty, A. A., Keeney, N., Cabaj, A., Kushner, P., & Bagnardi, M. (2022). Winter arctic sea ice thickness from icesat-2: upgrades to freeboard and snow loading estimates and an assessment of the first three winters of data collection. *The Cryosphere Discussions*, 1–40.

Petty, A. A., Kurtz, N., Kwok, R., Markus, T., & Neumann, T. A. (2022). *Icesat-2 l4 along-track sea ice thickness, version 1. [indicate subset used]* (Tech. Rep.). doi: 10.5067/JTI5YG3S6VAJ. [Accessed 18 Jan 2022].: Boulder, Colorado USA. NASA National Snow and Ice Data Center Distributed Active Archive Center.

Petty, A. A., Kurtz, N. T., Kwok, R., Markus, T., & Neumann, T. A. (2020). Winter arctic sea ice thickness from icesat-2 freeboards. *Journal of Geophysical Research: Oceans*, *125*(5), e2019JC015764.

Roach, L., Horvat, C., Dean, S. M., & Bitz, C. M. (2018). An emergent sea ice floe size distribution in a global coupled ocean – sea ice model. *J. Geophys. Res. Ocean.*.

Roberts, A. F., Hunke, E. C., Kamal, S. M., Lipscomb, W. H., Horvat, C., & Maslowski, W. (2019). A variational method for sea ice ridging in earth system models. *Journal of Advances in Modeling Earth Systems*, *11*(3), 771–805.

Rothrock, D. A. (1975). The energetics of the plastic deformation of pack ice by ridging. *Journal of Geophysical Research*, *80*(33), 4514–4519.

Schramm, J. L., Flato, G. M., & Curry, J. A. (2000). Toward the modeling of enhanced basal melting in ridge keels. *Journal of Geophysical Research: Oceans*, *105*(C6), 14081–14092.

Smith, M. M., Holland, M., & Light, B. (2022). Arctic sea ice sensitivity to lateral melting representation in a coupled climate model. *The Cryosphere*, *16*(2), 419–434.

Thorndike, A. S., Rothrock, D., Maykut, G., & Colony, R. (1975). The thickness distribution of sea ice. *Journal of Geophysical Research*, *80*(33), 4501–4513.

Ungermann, M., Tremblay, L. B., Martin, T., & Losch, M. (2017). Impact of the ice strength formulation on the performance of a sea ice thickness distribution model in the a rctic. *Journal of Geophysical Research: Oceans*, *122*(3), 2090–2107.

Wadhams, P. (2000). *Ice in the ocean.* CRC Press.

Supporting Information for "Effects of increasing the resolution of the sea ice thickness distribution in a coupled climate model on Arctic and Antarctic sea ice"

Madison M. Smith[1], Marika M. Holland[2], Alek A. Petty[3], Bonnie Light[1],

David A. Bailey[2]

[1]Polar Science Center, Applied Physics Laboratory, University of Washington, Seattle, USA

[2]National Center for Atmospheric Research, Boulder, Colorado, USA

[3]Cryospheric Sciences Laboratory, NASA Goddard Space Flight Center, Greenbelt, MD, USA

Contents of this file

Introduction Figure S1 shows the change in sea ice thickness in both hemispheres in February associated with increasing the ITD category resolution from 5 to 15 categories. Figures S2 to S6 show comparisons of ITD histograms from model runs and ICESat-2 derived thicknesses for all other regions not included in the manuscript. Figures S7 to S11 show comparisons of the ITD mean annual cycle for all other regions not included in the manuscript.

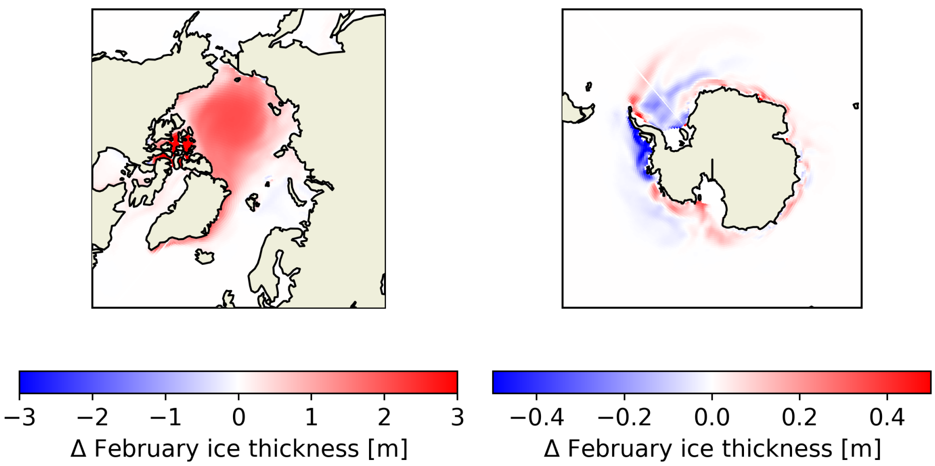

Figure S1. Difference in grid-averaged February sea ice thickness in the Arctic (left) and Antarctic (right) between run with 15 categories and 5 categories. Red indicates an increase in ice thickness with higher ITD category resolution, and blue indicates a decrease in ice thickness. Note that the scale of colorbar changes between panels.

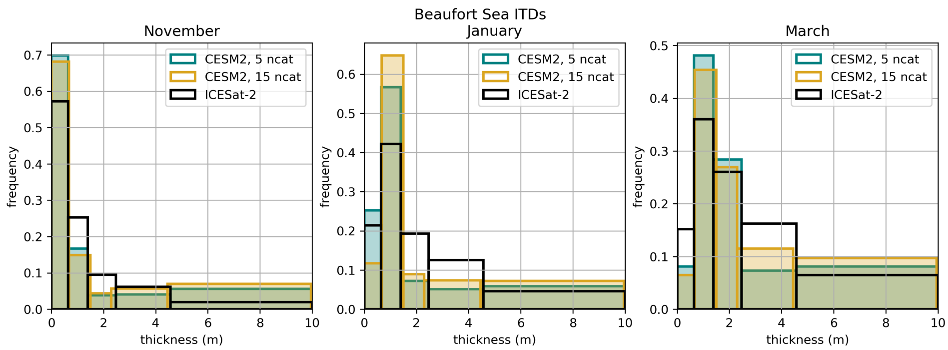

Figure S2. Comparison of discretized ice thickness distribution in the Beaufort Sea in model simulations and ICESat-2 for select months: November, January, and March. The average fraction of ice coverage in each category is shown for the 5 category model run (green), 15 category model run (gold), and ICESat-2 (black outline).

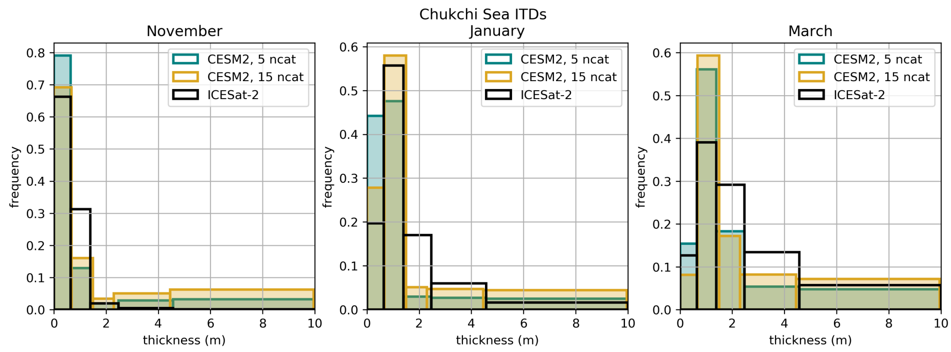

Figure S3. Comparison of discretized ice thickness distribution in the Chukchi Sea in model simulations and ICESat-2 for select months: November, January, and March. The average fraction of ice coverage in each category is shown for the 5 category model run (green), 15 category model run (gold), and ICESat-2 (black outline).

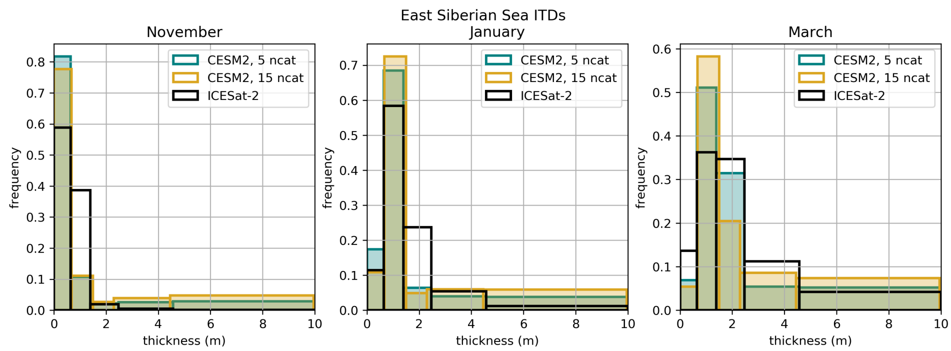

Figure S4. Comparison of discretized ice thickness distribution in the East Siberian Sea in model simulations and ICESat-2 for select months: November, January, and March. The average fraction of ice coverage in each category is shown for the 5 category model run (green), 15 category model run (gold), and ICESat-2 (black outline).

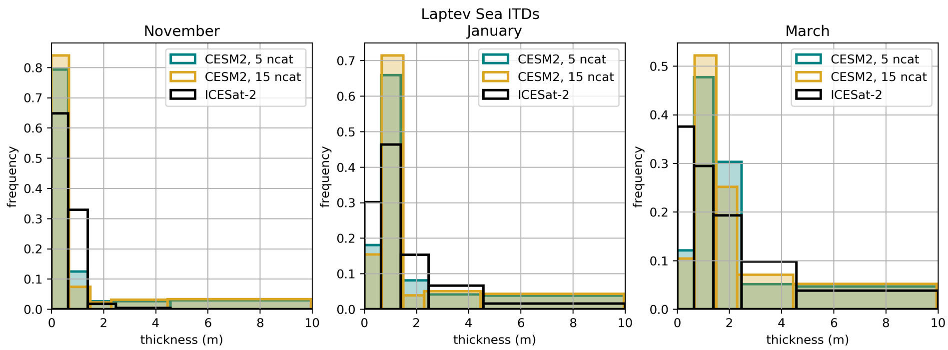

Figure S5. Comparison of discretized ice thickness distribution in the Laptev Sea in model simulations and ICESat-2 for select months: November, January, and March. The average fraction of ice coverage in each category is shown for the 5 category model run (green), 15 category model run (gold), and ICESat-2 (black outline).

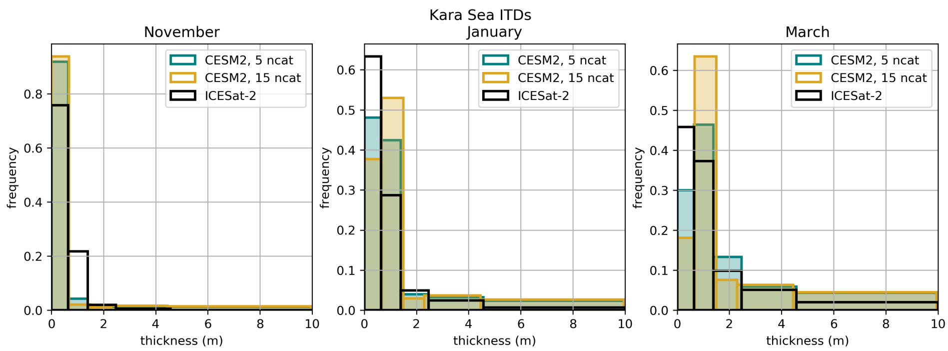

Figure S6. Comparison of discretized ice thickness distribution in the Kara Sea in model simulations and ICESat-2 for select months: November, January, and March. The average fraction of ice coverage in each category is shown for the 5 category model run (green), 15 category model run (gold), and ICESat-2 (black outline).

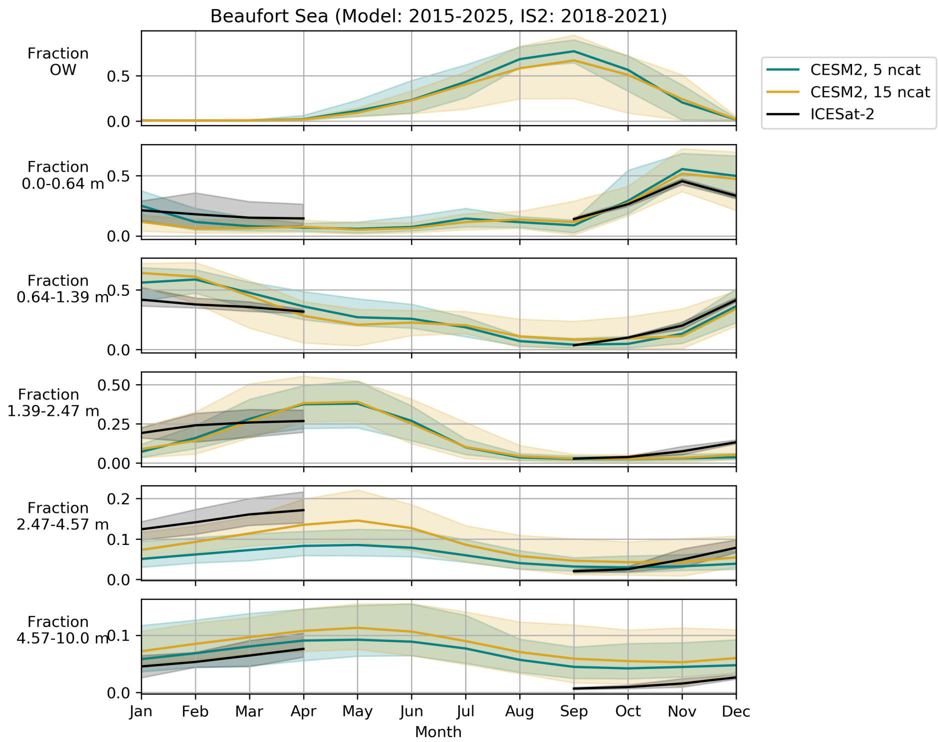

Figure S7. Mean annual cycle of the ice thickness distribution in the Beaufort Sea in model simulations and ICESat-2 observations. The fractional coverage of open water and in each ice category is shown for the control 5 category model run (green), 15 category model run (gold), and ICESat-2 (black). Shading represents the full range of values over the 10 years analyzed from the model or the 3 years of observations.

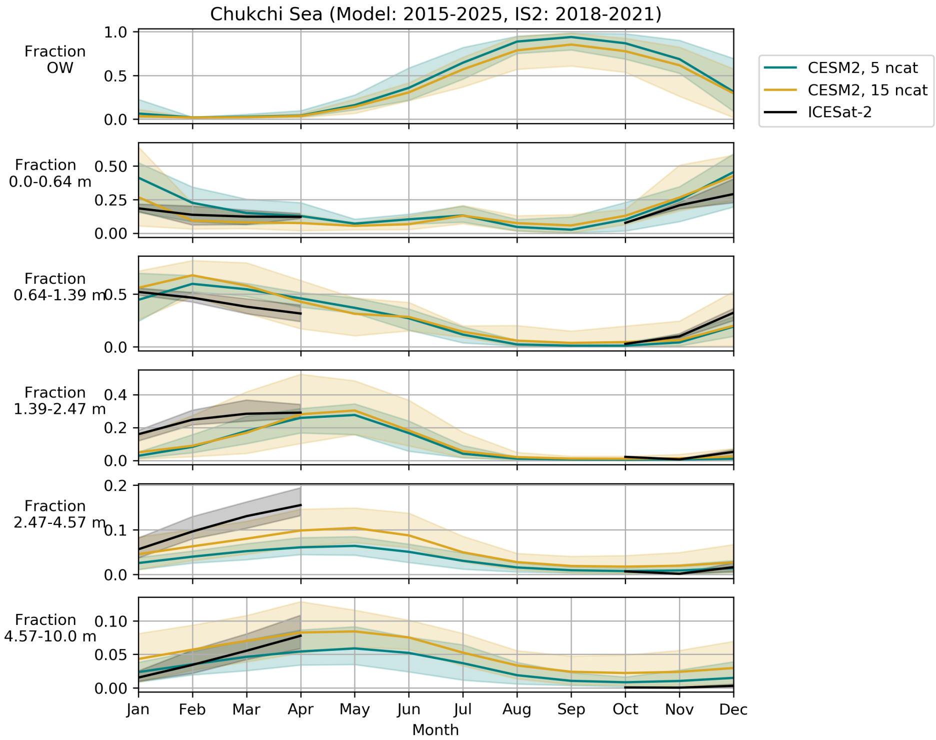

Figure S8. Mean annual cycle of the ice thickness distribution in the Chukchi Sea in model simulations and ICESat-2 observations. The fractional coverage of open water and in each ice category is shown for the control 5 category model run (green), 15 category model run (gold), and ICESat-2 (black). Shading represents the full range of values over the 10 years analyzed from the model or the 3 years of observations.

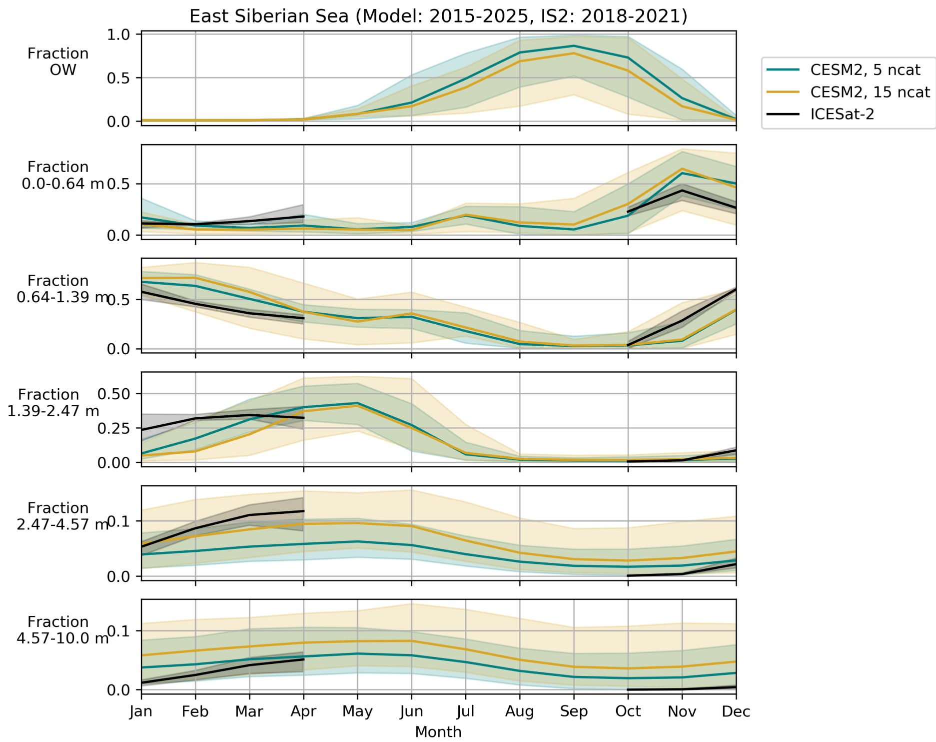

Figure S9. Mean annual cycle of the ice thickness distribution in the East Siberian Sea in model simulations and ICESat-2 observations. The fractional coverage of open water and in each ice category is shown for the control 5 category model run (green), 15 category model run (gold), and ICESat-2 (black). Shading represents the full range of values over the 10 years analyzed from the model or the 3 years of observations.

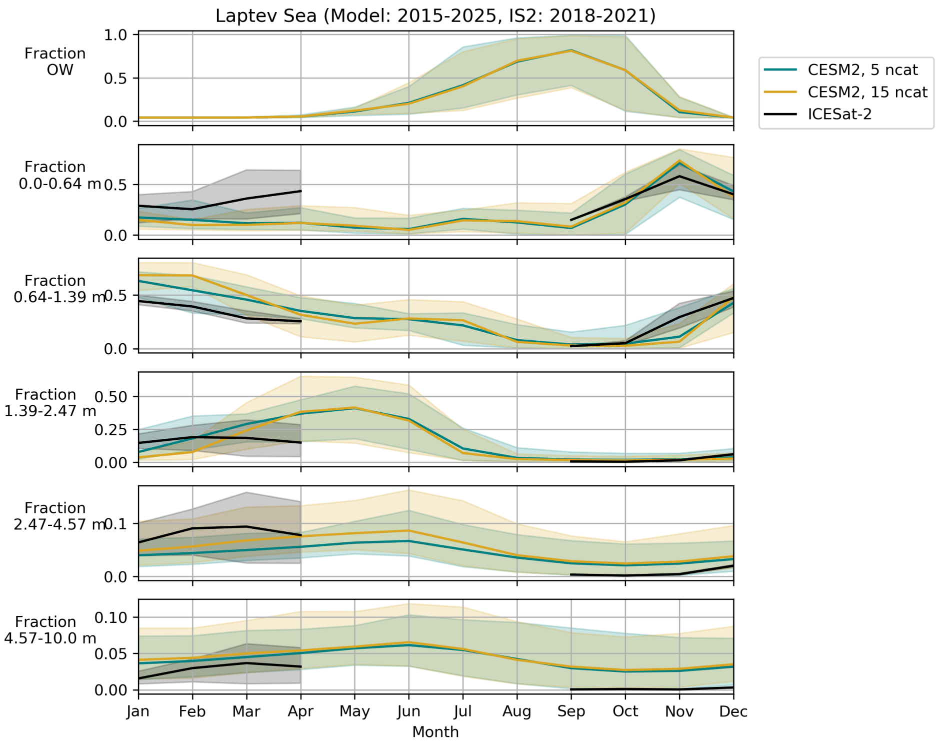

Figure S10. Mean annual cycle of the ice thickness distribution in the Laptev Sea in model simulations and ICESat-2 observations. The fractional coverage of open water and in each ice category is shown for the control 5 category model run (green), 15 category model run (gold), and ICESat-2 (black). Shading represents the full range of values over the 10 years analyzed from the model or the 3 years of observations.

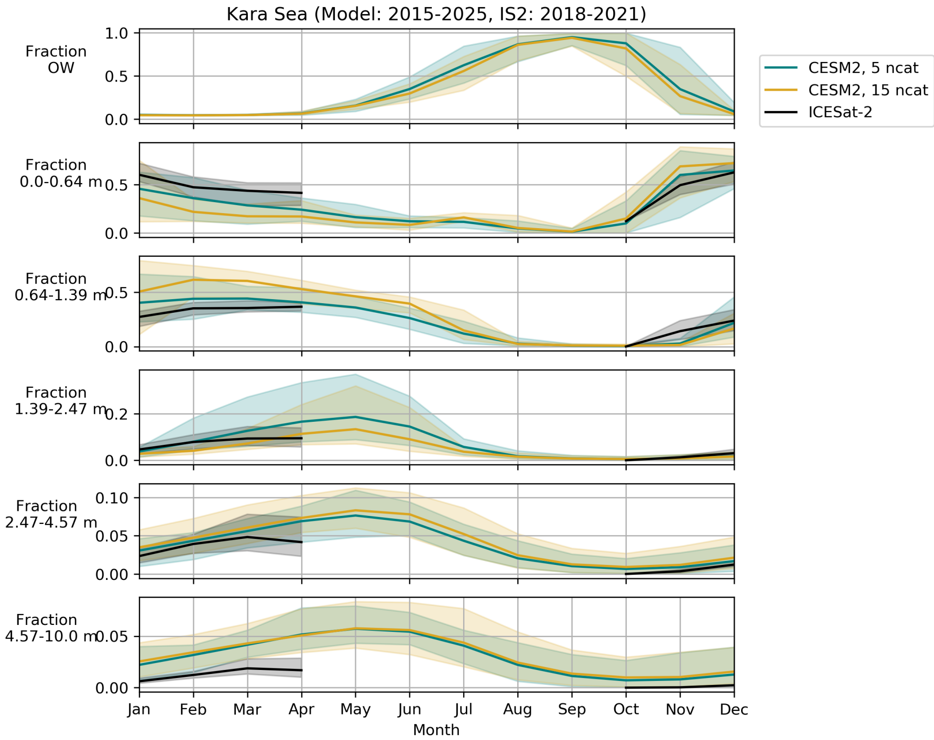

Figure S11. Mean annual cycle of the ice thickness distribution in the Kara Sea in model simulations and ICESat-2 observations. The fractional coverage of open water and in each ice category is shown for the control 5 category model run (green), 15 category model run (gold), and ICESat-2 (black). Shading represents the full range of values over the 10 years analyzed from the model or the 3 years of observations.